TRENDS IN SCIENCES 2025; 22(9): 10340
https://doi.org/10.48048/tis.2025.10340 RESEARCH ARTICLE

A Green Approach to N, S-doped Carbon Dots from Jengkol Peel (*Archidendron pauciflorum*) for Ratiometric Sensing of Amaranth Dye

Marpongahtun[1,*], Amir Hamzah Siregar[1], Agus Rimus Liandi[2], Amru Daulay[3], Salmiati[4], Aniza Salviana Prayugo[5] and Ririn Annisa[6]

[1]*Department of Chemistry, Faculty of Mathematics and Natural Sciences, University of North Sumatra, Medan, Indonesia*
[2]*Department of Chemistry, Faculty of Mathematics and Natural Sciences, Syarif Hidayatullah State Islamic University, Banten, Indonesia*
[3]*Research Center for Mining Technology, National Research and Innovation Agency (BRIN), Lampung, Indonesia*
[4]*Department Environmental Engineering, Faculty of Engineering, University of North Sumatra, Medan, Indonesia*
[5]*Postgraduate School, Department of Chemistry, Faculty of Mathematics and Natural Sciences, University of North Sumatra, Medan, Indonesia*
[6]*Graduate School, Department of Chemistry, Faculty of Mathematics and Natural Sciences, Universitas Sumatera Utara, Medan, Indonesia*

([*]Corresponding author's e-mail: marpongahtun@usu.ac.id)

Received: 10 April 2025, Revised: 30 April 2025, Accepted: 7 May 2025, Published: 10 July 2025

Abstract

The development of environmentally safe and cost-effective carbon nanoparticle-based ratiometric fluorescence sensors is critical for identifying hazardous synthetic food dyes. N, S-doped carbon dots (N, S-CD) were synthesized via a simple hydrothermal method using jengkol peel waste as the carbon source, with sodium thiosulfate and urea as co-dopants. The material exhibited spherical morphology with an average diamter 7.41 nm and a quantum yield of 20.5 %. Structural analysis confirmed the presence of graphitic structures containing hydroxyl, carboxyl, nitrogen, and sulfur functional groups on the particle surface, which improved dispersibility and created a conjugate system for fluorescence emission. With ideal emission/excitation peaks at 515/370 nm, N, S-CD exhibits excitation-dependent fluorescence. This N, S-CD based sensor has a detection limit of 7.5 nM (range 2.5 - 20 μM) and responds to amaranth with dual-emission fluorescence (λem 515/646 nm, λex 370 nm) through a FRET process. Validation on food samples revealed 94 - 98 % recovery, demonstrating the potential of biomass-based sensors for food safety analysis.

Keywords: Amaranth dye detection, Carbon dots, Jengkol peel, Food safety analysis, FRET mechanism, Nitrogen and sulfur co-dopants, Ratiometric fluorescence probe

Introduction

Food safety is a global concern, particularly azo dyes such as Amaranth (E123) in food and beverage products. Although effective as a colorant, Amaranth can cause liver damage and bladder cancer [1]. The limitations of current detection methods inhibit the monitoring of Amaranth levels in food products, thus potentially endangering consumer health. Various methods have been developed to detect Amaranth, such as absorption spectroscopy, chromatography, and electrochemical methods. However, these methods have limitations in terms of low sensitivity and complicated preparation [2].

Carbon Dots (CD) have emerged as a promising alternative as they are zero-dimensional carbon nanoparticles under 10 nm in size and are capable of fluorescence in various colors [3]. The fluorescence

ability is related to the structure of the carbon core surrounded by functional groups, giving it unique properties such as high water solubility and good response to the environment [4]. To improve the performance of CD, many doping techniques have been developed.

The co-doping of nitrogen and sulfur on CD has the potential to improve the fluorescence performance, where the enhancement mechanism depends on the electrons trapped in the N state and the modification of the electronic structure of CD [5]. Meanwhile, the addition of sulfur increases the density of states so that the excited electrons can increase the fluorescence intensity [6]. In recent developments, N, S-CD have been successfully used as fluorescence sensors for azo dyes including amaranth, with a ratiometric approach that provides the advantage of using the ratio of 2 emissions at different wavelengths, thus providing internal calibration and improving detection accuracy **[7].**

Although N, S-CD sensors have shown potential, the development of sensors with better performance is still needed. The biomass source used for CD synthesis greatly affects its characteristics and performance [8]. Jengkol peel is a biomass waste that contains a lot of nitrogenous heterocyclic organic compounds [9,10] has great potential for N, S-CD synthesis but has never been explored. The high nitrogen content in the jengkol peel is expected to increase the fluorescence intensity and stability due to its ability to bind the CD core. In addition, CD synthesized from biomass generally have better optical properties and are environmentally friendly compared to semiconductor quantum dots [11].

This study proposes the development of an N, S-CD based ratiometric fluorescence sensor using jengkol peel as a biomass source. This approach not only offers sensor performance content in the jengkol peel but is also in line with the principle of green chemistry, as it utilizes biomass waste for detecting amaranth.

Materials and methods

Material

Jengkol peel was obtained from Sumatera Utara Province, Indonesia, Aquadest, Deionisasi water, Urea (CH_4N_2O), natrium tiosulfat ($Na_2S_2O_3$), amaranth (95 %), nickel (II) nitrate hexahydrate ($Ni(NO_3)_2$), mercury(II) nitrate ($Hg(NO_3)_2$, copper (II) nitrate ($Cu(NO_3)_2$, cobalt (II) nitrate ($Co(NO_3)_2$, iron (II) nitrate ($Fe(NO_3)_2$, manganese (II) nitrate ($Mn(NO_3)_2$, zinc (II) nitrate ($Zn(NO_3)_2$, natrium chloride (NaCl), ascorbic acid, caffein, citric acid, glucose, tartazine, rhodamine blue were acquired from Sigma-Aldrich. All chemical com-pounds were utilized unpurified as received and belonged to the grade of analytical reagents.

Synthesis of carbon dots (CD)

The Jengkol peel is dried out and then powdered. The 10 g of jengkol peel powder was dissolved in 50 mL of deionized water. Subsequently, the liquid was poured into a 100 mL Teflon autoclave and heated at 220 °C for 7 h. The Whatman filter paper was used to filter the resulting dispersion and centrifuged at 10,000 rpm for 15 min to yield a brown solution. The obtained supernatant was then purified through a dialysis process using a membrane with a molecular weight cut-off of 10,000 DA for 24 h. The final product from this process was named CD.

Synthesis of nitrogen and sulphur co-doped carbon dots (N, S-CD)

Firstly, 10 g of jengkol peel powder, 5 g of urea, and 5 g of sodium thiosulfate were weighed and mixed in 50 mL of deionized water. Subsequently, the mixture was poured into a 100 mL Teflon autoclave and heated at 220 °C for 7 h. The Whatman filter paper was used to filter the resulting dispersion and centrifuged at 10,000 rpm for 15 min to yield a brownish-yellow solution. The obtained supernatant was then purified through a dialysis process using a membrane with a molecular weight cut-off of 10,000 DA for 24 h. The final product from this process was named N, S-CD.

The fluorescence measurements of amaranth dye by N, S-CD

N, S-CD were synthesized as sensor probes to detect amaranth dye. The selectivity and sensitivity of amaranth dye were investigated based on the fluorescence quenching efficiency at 370 nm. Experimental solutions were prepared as different control substances, such as amaranth (95 %), sodium chloride (NaCl), ascorbic acid, caffeine, citric acid, glucose, tartazine, rhodamine blue, and 7 different metal ions (Ni^{2+}, Hg^{2+}, Fe^{2+}, Mn^{2+}, Cu^{2+}, Co^{2+} and Zn^{2+}). The

N, S-CD solution (2 mL) was added with each at a concentration of 100 μM. The sensitivity of amaranth dye was examined further by incorporating amaranth concentration from (2.5 - 20 μM) into 2 mL of N, S-CD solution. Subsequently, fluorescence emission spectra were obtained, and the intensity of the emission peak was noted in the ambient.

N, S-CD on amaranth dye was tested on actual samples such as tomato juice and strawberry syrup. Samples of 15 mL were centrifuged for 30 min at 3,500 rpm. The supernatant was filtered using a 0.22 μM filtration membrane and diluted ten times with deionized water. Then, 2 mL of the resulting filtrate was spiked with several concentrations of amaranth and stirred for 10 min after adding 2 mL of N, S-CD solution. The actual concentration of amaranth was obtained through the measured fluorescence intensity.

Quantum yield measurement

Quantum yield (QY) investigation on CD and N, S-CD utilizing the equation that follows (1), Quinine sulfate dissolved in 0.1 M H_2SO_4 (QY = 54 % and η = 1.33) at 360 nm, used as reference [12].

$$\mathrm{QYc} = QYs \times \frac{Ic}{Is} \times \frac{As}{Ac} \times \left(\frac{\eta c}{\eta s}\right)^2 \quad (1)$$

where the quantum of yield represents QY, it relates to the brightness of the emission fluorescence. A signifies the absorbance t measured under the excitation wavelength, and η represents the solvent refractive index. C dan S, respectively for N, S-CD, and quinine sulfate. The photoluminescence spectrum was acquired with a Fluorescence Spectrometer

Results and discussion

Morphology, structure, and optical properties of CD and N, S-CD

Carbon dots were synthesized rapidly and environmentally friendly through the hydrothermal method. That treatment can dehydrate and decarboxylate the jengkol peel precursor to generate sp^2/sp^3 hybridization domains and various surface states on N, S-CD. Characterization results from TEM analysis in **Figures 1(a)** and **1(b)** show that CD and N, S-CD have a spherical particle morphology without aggregation, with an average size of 4.47 nm for CD and 7.41 nm for N, S-CD based on measurements of 100 particles. The increase in particle size in N, S-CD compared to CD indicates the successful doping of nitrogen and sulfur which enhances the nucleation activity and facilitates the formation of larger particles [13]. The findings support previous research showing N,S co-doping increases CD particle size, which is favorable for sensor applications because it provides a larger surface area for interaction with analytes [14].

XRD analysis (**Figure 1(c)**) confirmed the amorphous structure of CD with a broad peak (002) at 2θ = 24.02 ° [15], while N, S-CD showed increased crystallinity characterized by a sharp diffraction peak (002) at 2θ = 28.41 ° (FWHM = 0.14210) [16] and a lattice spacing of about 0.34 nm. The increase in crystallinity indicates that N, S co-doping not only affects the particle size but also induces the formation of sp^2 which contributes to the enhancement of graphitization and polycrystalline nature of carbon. These structural characteristics play an important role in improving the fluorescence properties of N, S-CD, This contrasts with earlier studies where CD exhibited amorphous structures [17].

XPS analysis revealed the successful modification of the CD structure through the doping process. CD in **Figure 2(a)**, shows the content of C1s and O1s (53.8 and 46.2 %) with characteristic peaks at 284.58 and 531.87 eV, as well as 3 main bond types at C1s resolution: C-C/C=C (284.58 eV), C=O (286.50 eV) [18]. **Figure 2(b)** reveals that N, S doping led to the incorporation of nitrogen (9 %) and sulphur (16.8 %), confirmed by absorption peaks at 163.67 eV (S2p) [19], 284.67 eV (C1s), 398.67 eV (N1s), and 531.67 eV (O1s). Resolution of C1s on N, S-CD showed the formation of new bonds at 284.67 eV (C=C/C-C), 285.4 eV (C-N/C-S), 287.3 eV (C=O), and 291 eV (C(O)-O), with an N1s peak at 398.67 eV from N pyrrolate and N pyridine confirming the formation of amino groups [20], while the S2p bond energy value indicates the presence of C-S-C bonds [21]. The high doping percentages demonstrate jengkol peel effectiveness as a nitrogen-rich precursor, resulting in N, S-CD with uniformly distributed dopants.

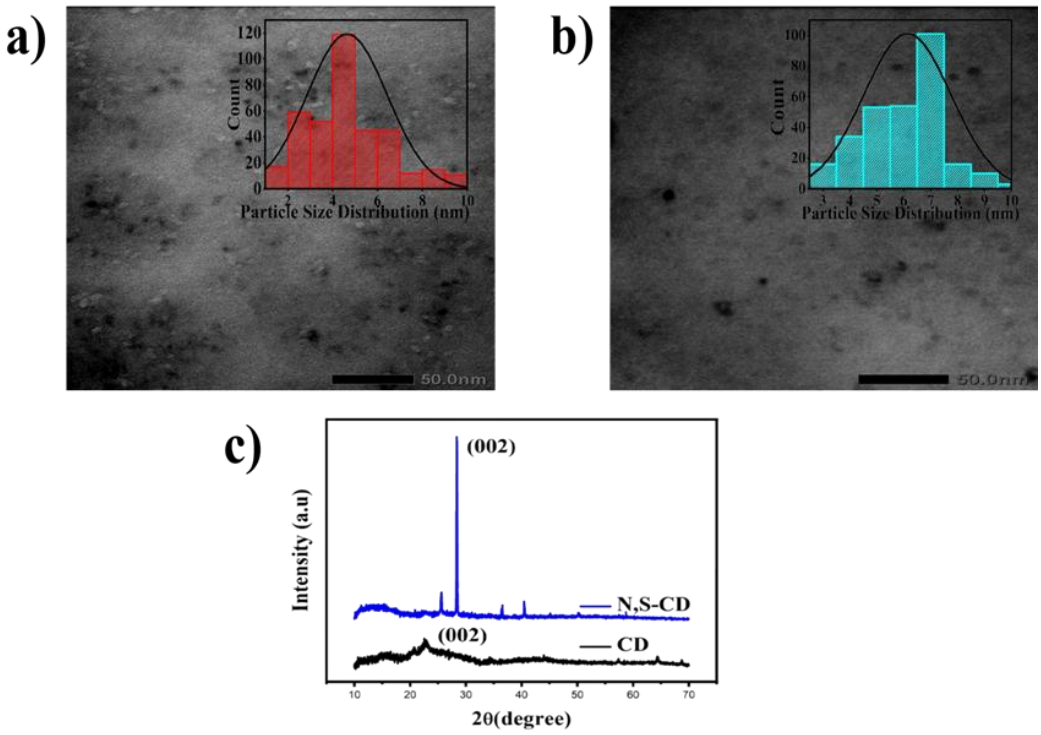

Figure 1 TEM images and inset of the size distribution of CD (a) and N, S-CD (b), and XRD spectra of CD and N, S-CD (c).

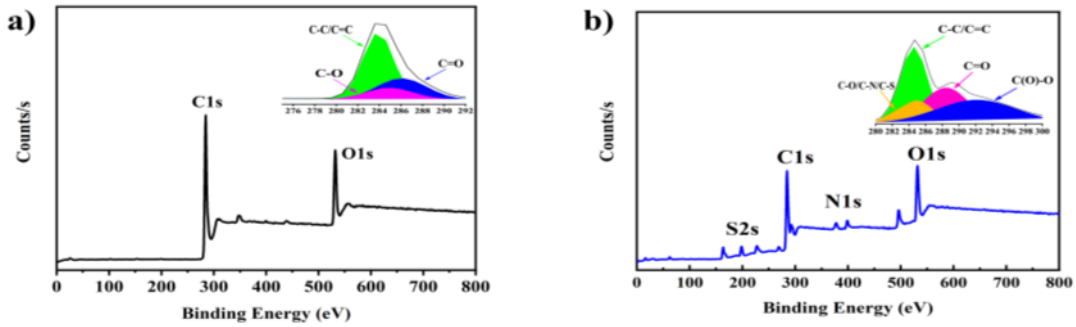

Figure 2 XPS spectra and high-resolution inset of C1s of CD (a) and N, S-CD (b).

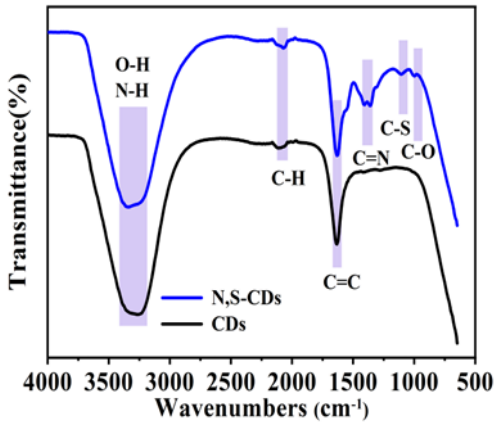

Figure 3 FTIR spectra of CD and N, S-CD.

FTIR spectra of N, S-CD, and CD (**Figure 3**) showed absorption bands at 3,231, 3,369 and 1,647 cm^{-1} (OH, N-H, C-H and C=H/C=C groups) [21]. These hydrophilic groups facilitate water dispersibility and create an optimal conjugation system for fluorescent emission [22]. The N, S-CD spectrum shows peaks at 1,412, 1,162 and 1,001 cm^{-1}, corresponding to C-N, C-S, and C-O-C vibrations, which confirms nitrogen and sulfur incorporation into the sp^2 carbon skeleton [23].

UV-Vis spectroscopy (**Figures 4(a)** and **4(b)**) reveals absorption band edges at 293 and 294 nm for CD and N, S-CD, respectively, attributed to π-π* transitions of C=C bonds. N, S-CD exhibits a distinct absorption at 348 nm due to n-π* transitions of CN, C=O, and CS bonds, where surface modification creates a p-conjugated structure leading to a red shift in fluorescence emission [24]. PL characterization (**Figures 4(a) and 4(b)**) reveals emission peaks at 462 nm (CD) and 515 nm (N, S-CD) with excitation wavelengths between 330 - 390 nm (**Figure 4(c)**). The redshift in emission wavelength accompanied by decreased PL intensity confirms N, S-CD excitation-dependent fluorescence properties [25].

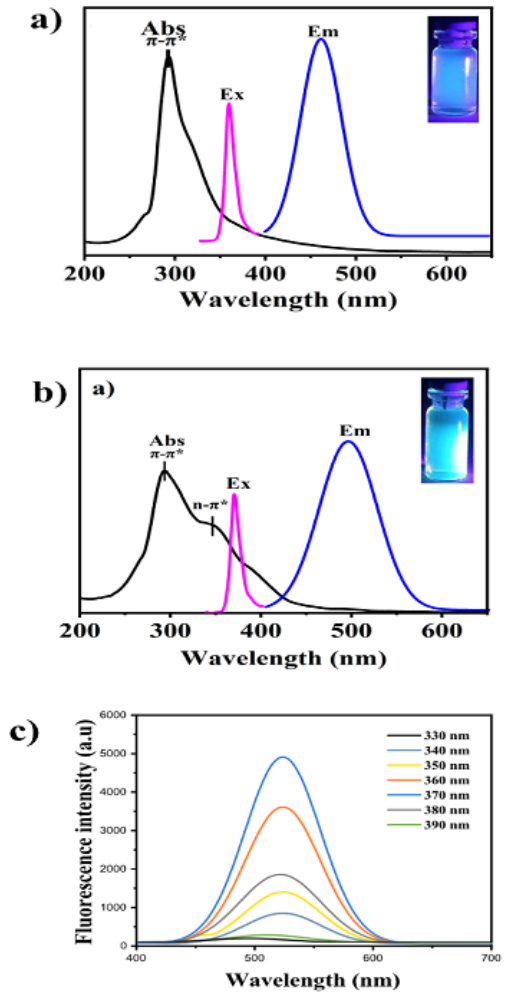

Figure 4 UV-visible spectra and PL spectra of (a) CD (b) N, S-CD. (c) excited N, S-CD (λex) with different wavelengths.

Excitation at 370 nm produces maximum intensity for both CD samples, where the N, S-CD surface functional groups facilitate the π-π* electronic transition at the C=C bond [26]. This transition process leads to emission variations from different surface states, primarily through interactions between reactive oxygen/nitrogen functional groups and the N, S-CD carbon skeleton, modifying the energy band gap. The functional groups act as energy traps on N, S-CD, influencing PL emission characteristics, evidenced by increased quantum efficiency from 4.5 % (CD) to 20.5 % (N, S-CD) through band gap narrowing. These

changes confirm successful optoelectronic property modification via doping.

Optimization of N, S-CD sensing parameters

Parameter optimization for amaranth sensing by N, S-CD was conducted through analysis of pH, ionic stability, luminescence performance, and photostability. Using a 100 μM amaranth solution, quenching efficiency was measured via the F0/F ratio. pH analysis (range 2 - 9) showed increasing fluorescence intensity from pH 2 to pH 7 (**Figure 5(a)**), indicating complex interactions between amaranth and N, S-CD through protonation and deprotonation.

In acidic conditions, protonation of oxygen groups on the surface of N, S-CD induces changes in energy levels that contribute to an increase in fluorescence intensity [27]. In contrast, at alkaline pH (8 - 9), deprotonation of functional groups resulted in a decrease in fluorescence response, confirming the critical role of proton balance in the sensing mechanism. The establishment of pH 7 as the optimal condition reflects the optimal balance between protonation and deprotonation for sensor-analyte interaction.

The analysis of N, S-CD storage stability in aqueous solution (**Figure 5(b)**) demonstrates excellent material durability, with fluorescence intensity maintained consistently throughout a 30-day period. This long-term stability indicates the strength of covalent bonds within the N, S-CD structure, which plays a crucial role in maintaining sensor integrity during storage.

Fluorescence response of N, S-CD to amaranth dye

Evaluation of the selectivity of N, S-CD (**Figures 6(a)** and **6(b)**) towards various interference components including NaCl, ascorbic acid, caffeine, citric acid, glucose, tartrazine, rhodamine blue, and 7 metal ions (Ni^{2+}, Hg^{2+}, Fe^{2+}, Mn^{2+}, Cu^{2+}, Co^{2+} and Zn^{2+}) revealed high selectivity towards amaranth. This selectivity occurs through the formation of hydrogen bonds between the hydroxyl/carboxylate groups of amaranth and the N/S groups on the N, S-CD surface, where the co-doped charge distribution favors electrostatic interactions and complex stability [28]. As a result of the interaction, there is a decrease in fluorescence intensity at 515 nm and an increase at 646 nm as the amaranth concentration increases (**Figure 6(c)**), indicating a resonance energy transfer mechanism that allows the development of a ratiometric detection system (F515/F646) in the range of 2.5 - 20 μM.

The change in intensity ratio is inversely proportional to amaranth concentration, marked by the color transition from cyan to yellow under UV excitation (**Figure 6(e)**), resulting in a detection limit of 7.5 nM with high linearity ($R^2 = 0.99$) can be shown in **Figure 6(d)**. The limit of detection (LOD) was estimated using:

$$LoD = 3\sigma/s \quad (2)$$

where σ represents the standard deviation of the blank (n = 3) and s is the slope of the linear curve.

This ratiometric method at 2 different wavelengths eliminates matrix interference and measurement fluctuations, providing better accuracy and reliability than conventional single intensity-based fluorescence methods [29]. The sensor performance comparison in **Table 1** confirms the effectiveness of the N, S-CD surface modification for azo dye detection over other carbon dot sensors.

Table 1 Literature review comparing the proposed research with other reports on amaranth and detection methods

Sensors	Analysis Method	Linear range	LOD (nM)	QY (%)	Ref
G-CD	Fluorescence	-	43.8	-	[31]
Carbon dots	Fluorescence	0.2 - 2.5 μM	19	-	[32]
S, N-CD	Fluorescence	0.2 - 30 μM	21	13	[33]
S, N-CD	Fluorescence	5 - 70 μM	345.22	10.90	[34]
Y/B-CD	Fluorescence	0.1 - 20 μM	42	0.75	[35]
N, S-CD	Fluorescence	2.5 - 20 μM	7.5	20.5	This work

Table 2 Investigation of amaranth in actual sample.

Sample	Spike (μM)	Detection (μM)	Recovery (%)	RSD (%, n = 3)
Strawberry syrup	1	0.4	94	0.6
	3	2.90	96	1.18
	5	4.90	98	0.5
Tomato juice	1	0.94	94	2.17
	3	2.88	96	1.74
	5	4.76	94	1.16

Analysis of fluorescence quenching mechanism

Analysis of the UV-Vis, emission, and excitation spectra of N, S-CD indicates fluorescence quenching by amaranth through FRET (Förster Resonance Energy Transfer) [30] . This is supported by the overlap between the emission spectrum of N, S-CD and the absorption spectrum of amaranth (**Figure 6(f)**), along with amaranth photoluminescence emission at 628 nm, which confirms that the emission at 646 nm originates from amaranth excited through FRET. In this mechanism, N, S-CD acts as an energy donor (intensity at 515 nm decreases), while amaranth as an acceptor produces an induced emission at ~650 nm whose intensity increases with amaranth concentration, demonstrating ratiometric characteristics with the F515/F646 ratio inversely proportional to amaranth concentration, confirming efficient resonance energy transfer.

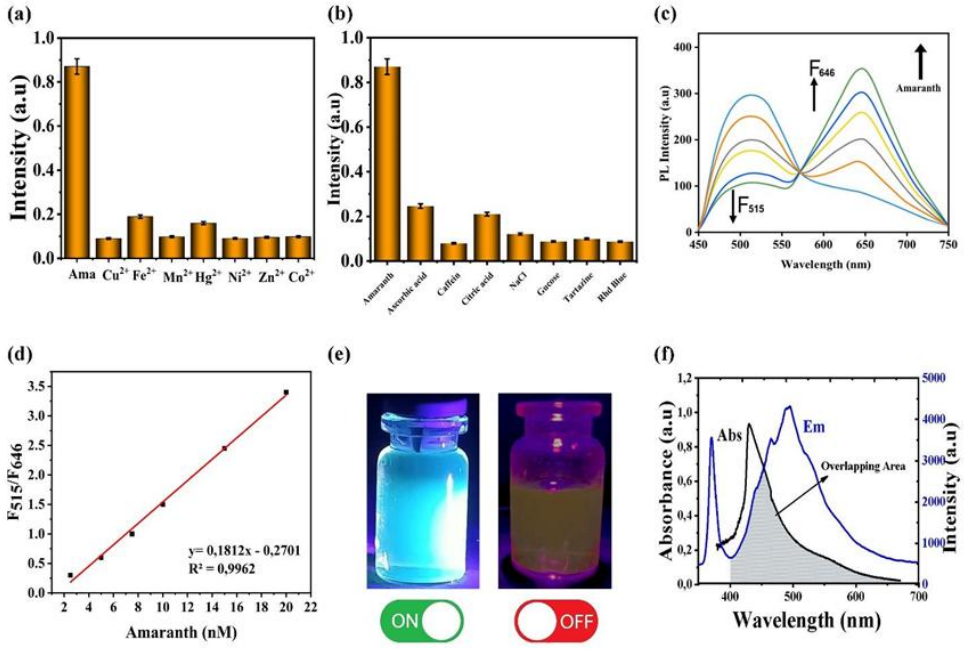

Figure 6 (a) and (b) fluorescence in various substances. (c) Fluorescence intensity decreases the spectrum of N, S-CD by adding amaranth concentration. (d) Relationship between F515/F646 and amaranth concentration. (e) Color emission shift from blue to yellow upon amaranth detection (f) Overlap scheme of N, S-CD spectrum.

Analysis by actual sample

Validation of the amaranth detection method in complex matrices using strawberry syrup and tomato juice as model food samples (**Table 2**) was carried out through the standard addition method at 3 concentrations (1, 3 and 5 μM). Testing in strawberry syrup resulted in 94 - 98 % amaranth recovery (RSD < 1.5 %), while in tomato juice it reached 94 - 96 % (RSD < 2.5 %). The high recovery rate and low RSD values

confirm the selectivity and reproducibility of the method in detecting amaranth in beverage matrices.

Conclusions

Ratiometric fluorescence probes were fabricated through surface modification of carbon dots using nitrogen and sulfur co-doping from the jengkol peel precursor via a 1-pot hydrothermal method with urea and sodium thiosulfate as dopants. The material exhibits spherical morphology with a 7.41 nm diameter and enhanced crystalline structure through N, S co-doping, achieving a 20.5 % quantum yield. The sensor produces a ratiometric response through interactions between N, S-CD surface functional groups, and amaranth via electron transfer mechanisms at dual wavelengths (emission/excitation 515/370 nm), with a linear detection range of 2.5 - 20 μM and 7.5 nM LOD. Its effective performance in real sample applications demonstrates the potential for developing biomass-based sensors for food safety analysis.

Acknowledgements

The authors gratefully acknowledge the support of Universitas Sumatera Utara (USU) in advancing the World Class University program. This work was supported by the Ministry of Research and Technology of the Republic of Indonesia with contract number 60/UN5.2.3.1/PPM/KP-WCU/2022.

Declaration of Generative AI in Scientific Writing

The authors acknowledge that generative AI (such as Quillbot and ChatGPT) was used in the preparation of this manuscript. The use of AI was for editing and grammar correction. No content was generated, nor was data interpreted using AI. All content and conclusions in this paper are based on our contributions and analysis.

CRediT Author Statement

Marpongahtun: Conceptualization, Methodology, Supervision, Validation, Funding acquisition, and Writing –original draft.
Amir Hamzah: Formal analysis, Validation, Supervision and Investigation.
Agus Rimus Liandi: Formal analysis, Supervision and Investigation.
Amru Daulay: Formal analysis, Supervision, and Investigation.
Salmiati: Formal analysis, Investigation, Validation, and Visualization.
Aniza Salviana Prayugo: Methodology, Data curation and Writing –original draft
Ririn Annisa: Methodology, Data curation and Writing –original draft

References

[1] MM Silva, FH Reboredo and FC Lidon. Food colour additives: A synoptical overview on their chemical properties. applications in food products, and health side effects. *Foods* 2006; **11(3)**, 379.

[2] K Rovina, S Siddiquee and SM Shaarani. Toxicology, extraction and analytical methods for determination of Amaranth in food and beverage products. *Trends in Food Science & Technology* 2017; **65(1)**, 68-79.

[3] S Manzoor, A Dar, K Dash, V Pandey, S Srivastava, I Bashir and S Khan. Carbon dots applications for development of sustainable technologies for food safety: A comprehensive review. *Applied Food Research* 2023; **3(1)**, 100263.

[4] H Shabbir, E Csapo and M Wojnicki. Carbon quantum dots: The role of surface functional groups and proposed mechanisms for metal ion sensing. *Inorganics* 2023; **11(6)**, 262.

[5] S Munusamy, T Mandlimath, P Swetha, GA Sehemi, M Pannipara, S Koppala, P Shanmugam, S Boonyuen, R Pothu and R Boddula. Nitrogen-doped carbon dots: Recent developments in its fluorescent sensor applications. *Environmental Research* 2023; **231(1)**, 116046.

[6] H Shabbir, T Tokarski, D Ungor and M Wojnicki. Eco-friendly synthesis of carbon dot by hydrothermal method for metal ions salt identification. *Materials* 2021; **14(24)**, 7604.

[7] R Gui and H Jin. Dual-emitting fluorescence ratiometric nanoprobes of *in-vitro*/*in-vivo* pH from constructions to sensing, imaging and therapeutic applications. *Journal of Photochemistry and Photobiology C* 2024; **58(9)**, 100650.

[8] A Daulay, L Nasution, M Huda, M Amin, M Nikmatullah, Supiyani and Yusmiati. Green sources for carbon dots synthesis in sensing for food application: A review. *Biosensors Bioelectronics: X* 2024; **17(1)**, 100460.

[9] M Rahmayanti, AN Syakina, I Fatimah and T Sulistyaningsih. Green synthesis of magnetite nanoparticles using peel extract of Jengkol (*Archidendron pauciflorum*) for methylene blue adsorption from aqueous media. *Chemical Physics Letters* 2022; **803(1)**, 139834.

[10] GA Wardani, L Nuramalia, WT Wulandari and E Nofiyanti. Utilization of Jengkol peel (*Pithecellobium jiringa* (jack) prain) as lead (II) ions bio-sorbent with column method. *Jurnal Kimia Sains dan Aplikasi* 2020; **23(5)**, 160-166.

[11] X Yang, S Fu, A Basta and L Lucia. A true biomass standout: Preparation and application of biomass-derived carbon quantum dots. *BioResources* 2024; **19(6)**, 6838-6858.

[12] Z Yi, X Li, H Zhang, X Ji, W Sun, Y Yu, Y Liu, J Huang, Z Sarshar and M Sain. High quantum yield photoluminescent N-doped carbon dots for switch sensing and imaging. *Talanta* 2021; **222(1)**, 121663.

[13] M Wu, J Li, Y Wu, X Gong and M Wu. Design of a synthetic strategy to achieve enhanced fluorescent carbon dots with sulfur and nitrogen codoping and its multifunctional applications. *Small* 2023; **9(42)**, e2302764.

[14] A Saengsrichan, C Saikate, P Silasana, P Khemthong, W Wanmolee, J Phanthasri, S Youngjan, P Posoknistakul, S Ratchahat, N Laosiripojana and C Sakdaronnarong. The role of n and s doping on photoluminescent characteristics of carbon dots from palm bunches for fluorimetric sensing of Fe^{3+} ion. *International Journal of Molecular Science* 2022; **23(1)**, 5001.

[15] D Cai, X Zhong, L Xu, Y Xiong, W Deng, G Zou, H Hou and X Ji. Biomass-derived carbon dots: Synthesis, modification and application in batteries. *Chemical Science* 2025; **16(12)**, 4937.

[16] N Zheng, M Zhang, B Liu, J Tang, F Zhang and G Chen. Influence of nitrogen-boron-sulfur triple-doping on the fluorescence emission of carbon dots and their sensing detection of copper ions. *Process Safety and Environmental Protection* 2025; **198(2)**, 107184.

[17] DK Dang, VN Nguyen, Z Tahir, H Jeong, S Kim, HN Tran, S Cho, YC Park, JS Bae, CT Le, J Yoon and YS Kim. An efficient green approach to constructing adenine sulfate-derived multicolor sulfur- and nitrogen-codoped carbon dots and their bioimaging applications. *ACS Applied Materials & Interfaces Journal* 2023; **15(27)**, 32783-3279.

[18] Y Zhu, G Li, W Li, X Luo, Z Hu and F Wu. Facile synthesis of efficient red-emissive carbon quantum dots as a multifunctional platform for biosensing and bioimaging. *Dyes and Pigments* 2023; **215(1)**, 111303.

[19] M Hamid, S Humaidi, H Wijoyo, I Isnaeni, IR Saragi, C Simanjuntak, NHM Kaus, MMA Kechik, A Nurbillah, Y yaakob and TI Nasution. Solvothermal synthesized N-S doped carbon dots derived from cavendish banana peel (*Musa paradisiaca*) for detection of Fe(III) and Pb(II). *Case Studies in Chemical and Environmental Engineering* 2024; **10(1)**, 100832.

[20] Y Zhang, N Liu, J Huang, S Wang, T Qing, Z Peng and B Feng. N, s co-doped carbon dots for fluorescent and colorimetric dual-mode detection of Co(II) in actual water. *Journal of Industrial and Engineering Chemistry* 2024; **37(12)**, 122-131.

[21] RB Gonzalez-Gonzalez, LT Gonzalez, M Madou, CL Porras, SO Martinez-Chapa and A Mendoza. Synthesis, purification, and characterization of carbon dots from non-activated and activated pyrolytic carbon black. *Nanomaterials* 2022; **12(3)**, 298.

[22] S Gavalas and A Kelarakis. Towards red emissive systems based on carbon dots. *Nanomaterial* 2021; **11(8)**, 2089.

[23] FRM Diana, A Suratman, ET Wahyuni, M Mudasir and S Suherman. Development of N, S-CDs fluorescent probe method for early detection of Cr (VI) in the environment. *Chemical Papers* 2022; **76(12)**, 7793-7809.

[24] D Ozyurt, MA Kobaisi, RK Hocking and B Fox. Properties, synthesis, and applications of carbon dots: A review. *Carbon Trends* 2023; **12(3)**, 100276.

[25] R Pramudita, Marpongahtun, S Gea, A Daulay, M Harahap, YZ Tan, R Goei, ALY Took and MJ Molaei. Synthesis of fluorescent citric acid carbon dots composites derived from empty fruit bunches of palm oil tree and its anti-bacterial property. *Case Studies in Chemical and Environmental Engineering* 2022; **6(1)**, 100277.

[26] MJ Molaei. A review on nanostructured carbon

quantum dots and their applications in biotechnology, sensors, and chemiluminescence. *Talanta* 2019; **196(1)**, 456-478.

[27] SMS do Nascimento, AF Sonsin, CDA do ES Barbosa and EJS Fonseca. Study of the pH effect on the optical and morphological properties of S, N self-doped carbon dots applied as fluorescent anti-counterfeiting ink and pH sensor. *Nanotechnology* 2023; **34(36)**, 365708.

[28] H Xuan, OL Juan, W Ji, LF Ling, SZ Ming, ZC Yan and SA Ming. Ratiometric fluorescence sensor for protamine and heparin based on N,P-doped carbon dots and Eosin Y. *Journal of the Chinese Chemical* Society 2024; **71(1)**, 1084-1091.

[29] AM Alaseem, K Alhazzani, AZ Alanazi, SM Alsanad, OA Alkhamees, G Alasiri, MME Wekil and ABH Ali. Dual-modulation ratiometric fluorescence strategy for cobalt and topotecan detection using Red-Emissive carbon dots. *Microchemical Journal* 2024; **201(4)**, 110645.

[30] N Ullal, K Muthamma and D Sunil. Carbon dots from eco-friendly precursors for optical sensing application: An up-to-date review. *Chemical Papers* 2022; **76(10)**, 6097-6127.

[31] Q Hu, J Kuang, J Yuan, Y Feng and Z Cheng. Detection of amaranth and iron in foods by modified carbon quantum dots as a ratiometric fluorescence probe. *Chemistry Select* 2024; **9(2)**, e202303816.

[32] A Kaur and U Gupta. Spectrophotofluorometric study of amaranth with fluorescent carbon dots and its analytical application. *Asian Journal Chemistry* 2014; **26(12)**, 70-73.

[33] L Liu, Z Mi, H Li, C Li, Q Hu and F Feng. Highly selective and sensitive detection of amaranth by using carbon dots-based nanosensor. *RSC Advances* 2019; **9(45)**, 26315-26320.

[34] Y Xiang, Y Tu, L Jiang, L Yuan, Z Liu, Q Xie, X Xiong and F Song. Orange fluorescent dual-mode nanoprobe for selective and sensitive detection of amaranth based on S,N-Doped carbon dots. *Dyes and Pigments* 2022; **205(6)**, 110533.

[35] L Yuan, L Liu, Z Mi, M Chen, Y Bai, J Qin and F Feng. A ratiometric sensor based on dual-emission carbon dots sensitive detection of amaranth. *Spectrochimica Acta Part A: Molecular and Biomeecular Spectroscopy* 2023; **302(1)**, 123058.